

How to Entangle or Disentangle Gaussian States with Hong-Ou-Mandel Interference

Fabian Schlue,^{1,*} Patrick Folge,¹ Takefumi Nomura,² Philip Held,¹ Federico Pegoraro,¹
Michael Stefszky,¹ Benjamin Brecht,¹ Stephen M. Barnett,³ and Christine Silberhorn¹

¹*Integrated Quantum Optics, Institute for Photonic Quantum Systems (PhoQS), Paderborn University, Paderborn, Germany*

²*Department of Applied Physics, School of Engineering, The University of Tokyo, Tokyo, Japan*

³*School of Physics and Astronomy, University of Glasgow, Glasgow G4 8QQ, UK*

(Dated: February 11, 2025)

The interference of two indistinguishable photons from a photon pair on a balanced beam splitter, where each photon enters in one of the input ports, yields a maximally entangled N00N-state shared between the outputs of the beam splitter through Hong-Ou-Mandel interference. At the same time, interference between the two modes of a two-mode squeezed state – the generalized output of a parametric photon-pair source – yields two independent, hence separable, single-mode squeezed states. Notably, both experiments use the *exact same* experimental setup. We resolve this seeming contradiction by measuring photon-number resolved quantum interference of the two modes of a two-mode squeezed state from an engineered parametric down-conversion source and show that the notion of inseparability is a result of *post-selection* on the presence of photons. Indeed, the complete joint photon statistics including the vacuum component are separable, as expected from textbook calculations.

I. INTRODUCTION

Photonics is an appealing platform for the implementation of numerous quantum technologies, such as quantum metrology and sensing, quantum communication, quantum simulation, and quantum computation. Traditionally, due to the pronounced wave-particle duality of optical fields, quantum photonics has been conceptually approached from two directions: on the one hand, continuous variable quantum optics (CVQO) focuses on the field aspect of light and investigates field quadratures to reveal effects such as squeezing; while on the other hand, discrete variable quantum optics (DVQO) employs the particle aspect of light through photon counting methods. Although DVQO and CVQO have traditionally been considered independently, new hybrid approaches, ones that combine the tenets of CVQO and DVQO, require us to rethink these distinctions.

It has been demonstrated that these hybrid investigations are capable of revealing new effects and physics, providing an opportunity to further develop our understanding of quantum systems [1]. One high-impact example of such a hybrid system is Gaussian Boson Sampling (GBS), which combines both approaches by interfering squeezed states in a large Haar-random beam splitter network and counts photons at the output of the network [2, 3]. This hybrid approach has allowed for the demonstration of quantum advantage in two experimental realizations [4, 5].

Although large networks such as those used in GBS can provide extremely powerful and interesting platforms for testing fundamental physics, questions can already be asked at the smallest possible network scale, i.e. a single beam splitter with two inputs and two outputs. In

DVQO it is well known that two indistinguishable photons impinging on a balanced beam splitter will undergo so-called Hong-Ou-Mandel interference (HOMI) [6]. This results in the photons bunching in the output ports of the beam splitter, resulting in a two-photon N00N-state [7], a maximally entangled state. The indistinguishable photons required for demonstrating this effect can be generated with an engineered type-II parametric down-conversion (PDC) source [8]. On the other hand, CVQO tells us that such a source generates a two-mode squeezed vacuum state (TMSVS), when going beyond the single-photon pair picture [9]. Note that these states are also called Einstein-Podolsky-Rosen (EPR) states [10]. If the two modes of a TMSVS interfere on a balanced beam splitter, they are transformed into two independent single-mode squeezed vacuum states (SMSVS) that are squeezed along conjugate field quadratures. In fact, the reverse process (the interference of two SMSVS on a balanced beam splitter) is often used for the generation of TMSVSs [11, 12].

The above two statements seemingly contradict each other: if the DVQO picture is employed, a separable state becomes entangled, while the opposite is true in the CVQO picture. However, the underlying physics is the same in both cases. This hints to the fact that considering things holistically reveals inconsistencies and forces us to question the distinction between CVQO and DVQO.

In this work we take a holistic approach and treat the described system in a hybrid way. We will show that the differences between CVQO and DVQO perspectives originates from the observables they measure. CVQO is concerned with the field aspects and measures the complete field including the vacuum, while DVQO uses photon counting, mostly not measuring the complete field, but conditioning on the presence of photons (removing the vacuum component). Exactly this conditioning is what makes the DVQO treatment of this interference ex-

* fabian.schlue@upb.de

periment create entanglement, rather than a separable state.

We demonstrate this experimentally by detecting interference of the two modes of a TMSVS on a balanced beam splitter with photon-number resolving detectors, thus going beyond the usual HOMI setting. Our source generates a state that is a close approximation of an ideal textbook single spectral-mode TMSVS [9]. In addition, it features a high brightness, which enables the presence of significant higher photon number components for our analysis. For the photon-number resolution we employ time-multiplexed detection with 8 detection bins per beam splitter output. This allows us to measure photon-number correlations from the PDC interference up to 16th order.

Our goal is quantify the amount of correlation present in our joint photon number distribution. To this end, we compare three different criteria: firstly, the correlation coefficient, which is a statistical method for characterizing the amount of correlation between two variables. It is based on second-order correlations and therefore disregards higher-order correlations measured in this experiment. Secondly, the Schmidt number and thirdly the mutual information both consider also higher-order correlations. The Schmidt number is often used in DVQO, whereas the mutual information is a statistical measure often used in information processing.

We find that, when taking the complete joint probability distribution, including the vacuum component, the state in the two outputs of the beam splitter is, indeed, separable. When conditioning on the presence of photons, removing the vacuum component—corresponding to the archetypical Hong-Ou-Mandel interference—we find photon-number entanglement. In addition, we demonstrate that evaluating higher-order correlations provides better agreement with our simulations than only considering up to second-order correlations for gauging the amount of correlation present. This is unsurprising since higher-order correlations generally carry additional information [13]. Finally, we demonstrate that our method can directly assess the quality of the SMSVSs generated through the interference of a TMSVS, specifically by evaluating their separability. This is an important metric in the context of high-dimensional photonic networks, e.g. Gaussian boson sampling, which requires single spectral-mode SMSVS as a resource.

II. CONCEPT AND THEORY

The concept of this work is shown in FIG. 1. We begin with the phase space representation of a quadrature entangled TMSVS (FIG. 1 a), left). Here P_i and X_i for $i \in \{A, B\}$ correspond to the field quadrature amplitudes. The state is characterized by each individual mode having larger quadrature fluctuations $\langle(\Delta\hat{X}_i)^2\rangle$ and $\langle(\Delta\hat{P}_i)^2\rangle$ (blue area) than the vacuum (black dotted circle). However, the measurement of one subsystem al-

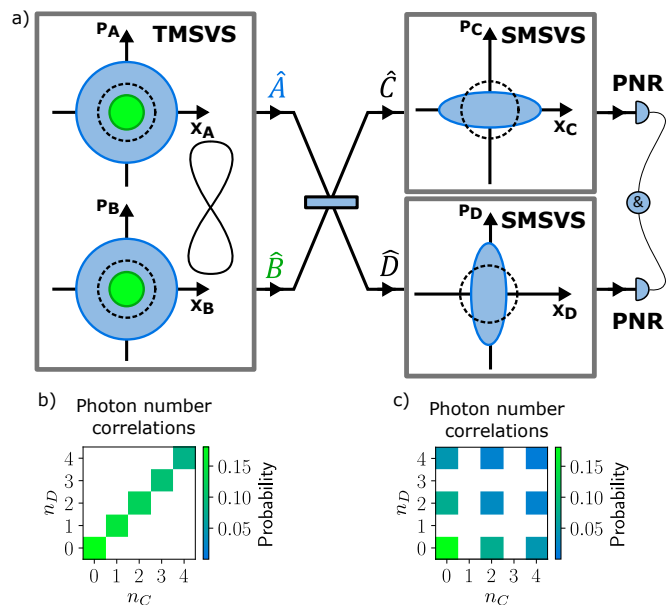


FIG. 1. Conceptual representation of the presented experiment. a) A TMSVS is interfered on a 50:50 beam splitter, resulting in two SMSVSs, P_i and X_i are field quadrature amplitudes in the respective beam splitter ports. The resulting photon number statistics are measured with a photon number resolving (PNR) detector. b) and c) Joint photon number distributions for a TMSVS and two SMSVSs, respectively, n_i is photon number in the respective output.

lows us to infer the properties of the second subsystem to below the quantum limit (green area), i.e. reduced conditional variance, or EPR entanglement [14].

Interfering the TMSVS on a 50:50 beam splitter will result in two independent, phase shifted, SMSVS [15], see FIG. 1 a), right panels. SMSVSs are characterized by exhibiting quadrature fluctuations below the vacuum level along one axis (squeezing) and fluctuations higher than the vacuum level along the orthogonal axis (anti-squeezing).

The resulting joint photon number distributions $P(n_C, n_D)$ for lossless TMSVS and two SMSVSs are shown in FIG. 1 b) and c). For more information see Appendix A.

In FIG. 1 b) one can clearly see perfect photon number correlations of the TMSVS. However, in FIG. 1 c) it may not be obvious that the joint photon number distribution of the two SMSVSs is separable. This differentiation becomes even harder in the realistic scenario that includes noise and losses.

To measure the amount of correlation we first introduce the correlation coefficient corr which is the normalized form of the covariance cov [16]

$$\text{corr}(X, Y) = \frac{\text{cov}(X, Y)}{\sigma_X \cdot \sigma_Y}, \quad (1)$$

where X and Y are two random variables and $\sigma_{X(Y)}$

are their respective standard deviations. The correlation coefficient is bounded between 1 and -1, indicating perfect correlations and anti-correlations respectively. When the random variables X and Y are completely uncorrelated the correlation coefficient is zero. Note that the correlation coefficient in Eq. (1) is sensitive only to the degree of second-order correlation [16]. Therefore, a state exhibiting higher-order correlations can have a correlation coefficient of 0. In the framework of CVQO it is common to focus on so-called Gaussian states, states that exhibit a Gaussian Wigner function. These are fully characterized by their first and second order moments, hence the correlation coefficient is well suited for evaluating properties of these states.

As a second method, we will utilize the Schmidt decomposition. In contrast to the correlation coefficient, this method is sensitive to higher-order correlations. In [17], the Schmidt decomposition for any pure quantum state $|\psi\rangle \in \mathcal{H} = \mathcal{H}_u \otimes \mathcal{H}_v$, which is a state of a composite system, is given by

$$|\psi\rangle = \sum_{i=0}^{\infty} g_i |u_i\rangle \otimes |v_i\rangle. \quad (2)$$

Here, the $\{|u_i\rangle\}$ and $\{|v_i\rangle\}$ form orthonormal bases of \mathcal{H}_u and \mathcal{H}_v , respectively, and $g_i \in \mathbb{C}$. In particular, the authors show that a TMSVS is decomposed as

$$|\psi\rangle_{\text{TMSVS}} = \hat{S}_{ij}(\xi) |0\rangle = \sum_{n=0}^{\infty} c_n |n\rangle_u \otimes |n\rangle_v, \quad (3)$$

where $\hat{S}_{ij}(\xi)$ is the two-mode squeezing operator in spatial modes i and j with squeezing parameter $\xi \in \mathbb{C}$ (see Eq. (C1)), the c_n are the complex amplitude coefficients, and the $|n\rangle$ are photon-number Fock states.

On the other hand, the Schmidt decomposition often appears in the context of photon-pair states generated in parametric down-conversion [18]. Here, we decompose the so-called joint spectral amplitude $f(\omega_s, \omega_i)$ that describes the spectral content of the PDC state as $f(\omega_s, \omega_i) = \sum_{i=0}^{\infty} \sqrt{\lambda_i} \psi_i(\omega_s) \phi_i(\omega_i)$, with the $\psi_i(\omega_s)$ and $\phi_i(\omega_i)$ describing the temporal modes [19] of signal and idler, respectively. The Schmidt decomposition yields a measure for the modal content of the photon-pair state, the so-called Schmidt number $K = 1 / (\sum_{i=0}^{\infty} |\lambda_i|^2)$. This number equals the effective number of spectral modes that the state occupies and simultaneously quantifies the spectral entanglement between the two photons. It ranges from $K = 1$ for a separable, spectrally single-mode state to $K \rightarrow \infty$ for a perfectly correlated and hence spectrally maximally entangled state.

In this work, we apply the notion of the Schmidt number to the case of Eq. (3), where the modes u and v now label the two output ports of the beam splitter C and D . We assume that the state to which we apply the Schmidt decomposition is spectrally single mode—a condition that holds true for the TMSVS resource generated by our source ($K = 1.3$)—and find that the Schmidt

number K is now a measure for the photon-number correlation between the two subsystems \mathcal{H}_u and \mathcal{H}_v . As a detail, note that we apply the Schmidt decomposition to the measured intensities instead of the amplitudes of the states. This is justified because phases between different photon-number components would not change the decomposition.

The third method we use is the mutual information $I(X, Y)$ [20]. This measure, like the Schmidt number, is sensitive to higher-order correlations and is often used in information sciences. It is defined as

$$I(X, Y) = \sum_{n_1, n_2} P(n_1, n_2) \log_{10} \frac{P(n_1, n_2)}{P(n_1)P(n_2)}, \quad (4)$$

where $P(n_1, n_2)$ is the joint photon number distribution and $P(i)$ is the respective marginal distribution of $P(n_1, n_2)$. The mutual information is always $I(X, Y) \geq 0$ and $I(X, Y) = 0$ if and only if $P(n_1, n_2) = P(n_1)P(n_2)$ is separable.

III. EXPERIMENT

We generate our TMSVS with a type-II PDC source in a 25mm long periodically poled potassium titanyl phosphate waveguide [21] (see FIG. 2). Due to careful dispersion engineering, the source generates a single spectral-mode, pulsed, spectrally degenerate TMSVS with very good approximation. We find an effective number of spectral-modes of 1.3. For this we make sure that the pump pulse spectral width is matched to the phase matching bandwidth [8, 22]. We verify this using the second order normalized correlation function measure $g^{(2)}(0)$ and achieved a value of 1.75 ± 0.05 , which is linked to the effective mode number [23]. Additionally, we verified a high interference visibility of the created photons in a HOMI experiment and reached 94% visibility, highlighting the exchange symmetry of the photons. In this work, this requires pump pulses with a duration of 3 ps and a central wavelength of 772.5 nm, which we derive from an ultrafast oscillator with a repetition rate of 76.4 MHz. We reduce the pulse repetition rate to 200 kHz using a pulse picker to facilitate time-multiplexed photon counting [24]. After the source we use a wavelength filter to suppress the pump light and a 1.8 nm wide spectral band-pass filter that is matched to the central peak in the generated spectrum. The band-pass filter removes phase matching sidebands which would increase the number of spectral modes [25] and is used in all presented measurements.

The high-quality photon pairs are split on a polarizing beam splitter (PBS) and interfere at the following balanced fiber beam splitter (BS). One output of the PBS possesses an adjustable delay, enabling variable temporal overlap between the two outputs of the PBS at the BS. In the other output of the PBS a half wave plate (HWP)

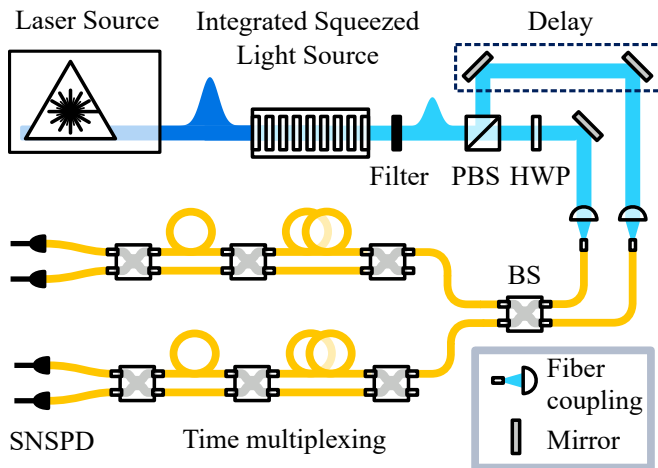


FIG. 2. Schematic representation of the experimental setup. An integrated squeezed light source is pumped by a pulsed laser. The resulting TMSVS is filtered and split on a polarizing beam splitter (PBS). The polarization of one output of the PBS is rotated by a half-wave plate (HWP) to interfere both outputs on a balanced fiber beam splitter (BS) with an adjustable delay. The click statistics are measured via time-multiplexed detection on superconducting nano-wire single photon detectors (SNSPD).

rotates the polarization of the created photons by 90° to ensure polarization indistinguishability at the BS.

The PNR in our experiment is achieved via two independent 8 time-bin time-multiplexed detectors (TMDs) [26]. The first TMD, hereafter referred to as the high efficiency arm, has a time-bin separation of 100 ns, compatible with a superconducting nano-wire single photon detector (SNSPD) system with 70 ns dead time and $> 90\%$ quantum efficiency. The second is optimized for speed and has a time-bin separation of 17 ns, compatible with an SNSPD system with 13 ns dead time and $> 70\%$ quantum efficiency, hereafter referred to as the low efficiency arm. One could have used a single TMD for the measurement of the joint photon number distributions, however, our devices lack a long fiber delay on the second input required to use both inputs. This results in slightly asymmetric efficiencies for the two measured outputs of the PDC. The total efficiencies are $20\% \pm 6\%$ and $14\% \pm 6\%$ for the high and low efficiency arm respectively. For more detail see Appendix B. The signals from the 4 SNSPDs are recorded using a time to digital converter. By calibrating the temporal delay between the reference laser trigger and the individual time bins of both TMDs we are able to narrowly time-filter the bins within a 2 ns window, thereby reducing noise counts. With this calibration we correlate the number of detection events in each output on a shot-by-shot basis to measure the joint click distribution of the input state with up to 8 detection events per output [27]. We measured the joint photon number distribution at different temporal overlaps of the input pulses at the fiber beam splitter, with each joint photon number distribution containing 228 million experimental

runs. We describe in the next section how we convert the measured data to the joint photon number distribution.

Obtaining high quality data requires one to carefully choose the operating power. We operated the source at a measured mean photon number of 0.060 ± 0.008 in the high efficiency arm. This corresponds to having $P(1, 1) = 6 \cdot 10^{-3}$, $P(2, 2) = 9 \cdot 10^{-5}$ and $P(3, 3) = 1 \cdot 10^{-6}$. This low mean photon number is far away from detector saturation effects. Note that we are operating in a regime where the DVQO approximation of low probability for higher photon numbers is often assumed and, therefore, they are neglected [28, 29]. However, we are explicitly measuring them and show their impact.

Significant fluctuations in the mean photon number were observed, due to laser instability. We scanned the configured delay (see delay axis in FIG. 3 a)) several times with shorter integration time, therefore, the power drifts are present in all configured delays of the measurement. The large dependence on the mean photon number will be discussed in the next section.

IV. RESULTS

The joint click statistics of the interference of a TMSVS at a BS with varying temporal overlap between the inputs was measured. First, the joint click statistics need to be converted to pseudo photon number correlations, due to the probabilistic nature of splitting the input pulse inside the TMD. There are ways of correcting for this so called convolution [30, 31], by using the fact that we know how likely it is to get multiple photons in one detection bin, assuming equal splitting in the TMD. To recover the photon number statistics we use the method presented in [31], which is applied to all data before proceeding with further analysis.

We compare our experimental results to simulations detailed in Appendix C. The simulation takes the measured squeezing strength and losses as input parameters. The squeezing strength r for a single spectral mode TMSVS is back-calculated from the measured mean photon number \bar{n} and losses η in the experiment via $r = \text{arsinh}(\sqrt{\bar{n}/\eta})$. The confidence region of our simulations is the standard deviation of the measured photon number, as it is the largest experimental uncertainty. We used the measured losses from the experiment and distribute the losses before and after the interference at the 50:50 beam splitter as measured in the experiment (see Appendix B). From this we obtain the joint photon number distribution and proceed with the same analysis as with the experimental data.

The results of our analysis can be seen in FIG. 3. In FIG. 3 a) the measured values for the three correlation measures and the results from their respective simulations are shown. In general one sees that all three correlation measures follow their respective simulations rather closely. We compare our measured data to a parameter-free theory based on an ideal TMSVS at the input of

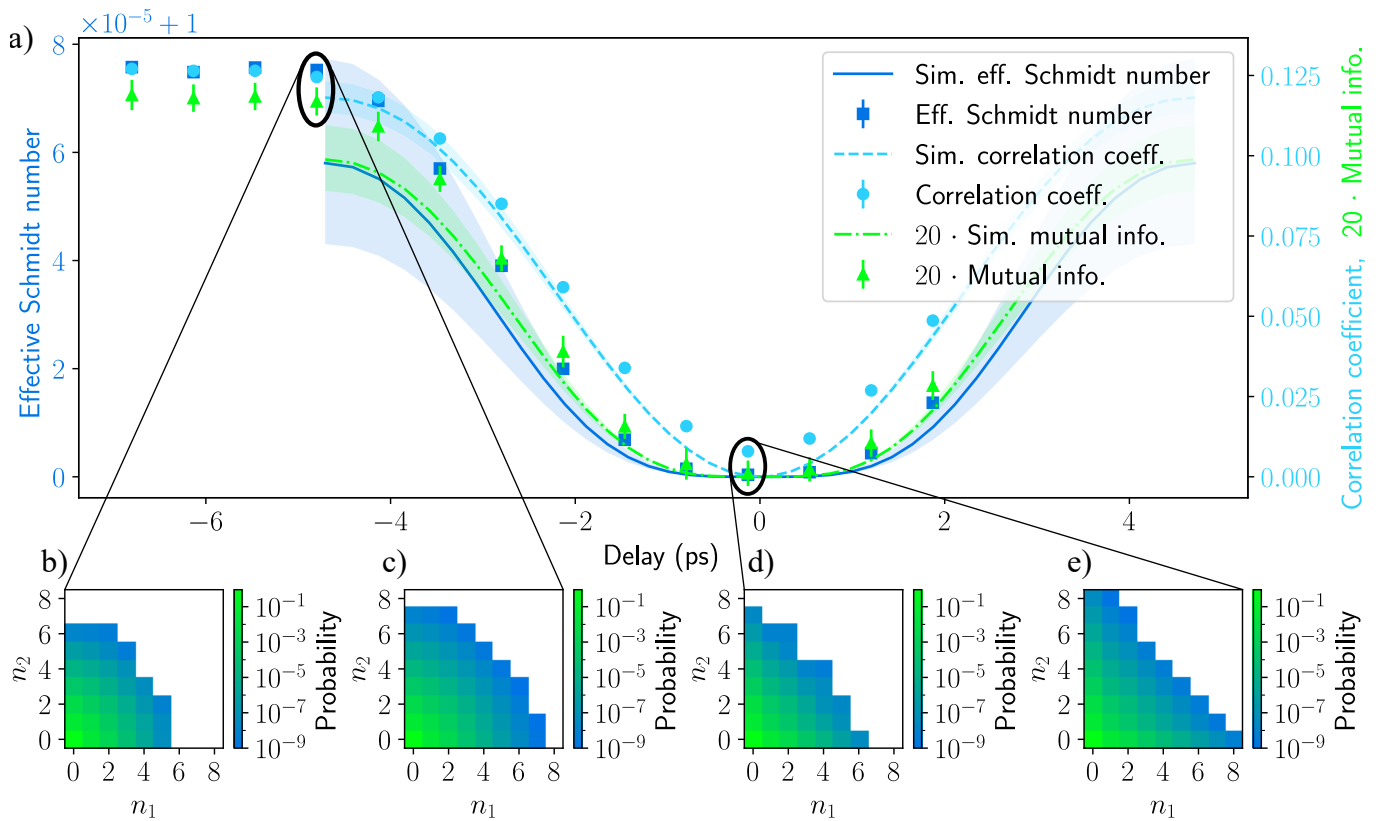


FIG. 3. a) Correlation measures as the temporal delay between the two pulses is varied. b) and d) measured joint photon number distribution for high and zero temporal delay as indicated in a), n_i photon number. c) and e) simulated joint photon number distribution corresponding to the same temporal overlaps as the measured distributions.

the beam splitter and only account for experimentally measured efficiencies. The good agreement between experiment and simulation is testimony to the high single mode quality of our source.

There are, however, some deviations of the measured values from the simulations. One deviation can be seen for temporal separations greater than -4 ps, there the experimental values are on the upper edges of the confidence intervals of the simulation. Another deviation is present for the correlation coefficient at zero time delay where the simulation and measurement do not overlap. We suspect that these deviations are caused by the slight spectral multimodedness of our PDC source that our simulation does not account for. Effects of multimodedness in HOMI experiments have been shown theoretically and in experiment [32].

All three correlation measures in FIG. 3 a) show correlations for temporal delays larger than -4 ps. This is consistent with the fact that at this temporal separation, the TMSVS pulses with duration of 3 ps do not exhibit a significant temporal overlap. Therefore, minimal interference takes place. In contrast, for a temporal delay of 0 ps, the value of the Schmidt number is very close to 1 and the mutual information is consistent with 0 inside the error margin, due to near perfect interference. This indicates that the outputs are very close to inde-

pendent, as one would expect in the ideal case of two independent squeezers. The correlation coefficient shows a similar shape as the other two measures, but does not go to 0. The main difference between the experiment and simulation is the missing spectral multimodedness in the simulation. This suggests that the correlation coefficient is more sensitive to the effects of multimodedness than the other two measures. As a side note, if this sensitivity can be shown in simulations, then the correlation coefficient might be an interesting new measure for the multimodedness in a HOMI experiment, which the HOMI is typically not directly sensitive to.

Another interesting property of the correlation coefficient, seen in both theory and measurements, is its higher sensitivity to pulse overlap of the input pulses, as the distributions are narrower (see FIG. 3 a)). This indicates that the correlation coefficient can be a better measure for finding the best temporal overlap in the measured joint photon number distributions [33]. However, one might need to be careful applying this method in highly multi-mode cases when only weak interference is present, due to the possible sensitivity of the correlation coefficient to multimodedness.

Next, we investigate the joint photon number distributions themselves, illustrated in FIG. 3 b) and d). These correspond to the regions as indicated in FIG. 3 a). One

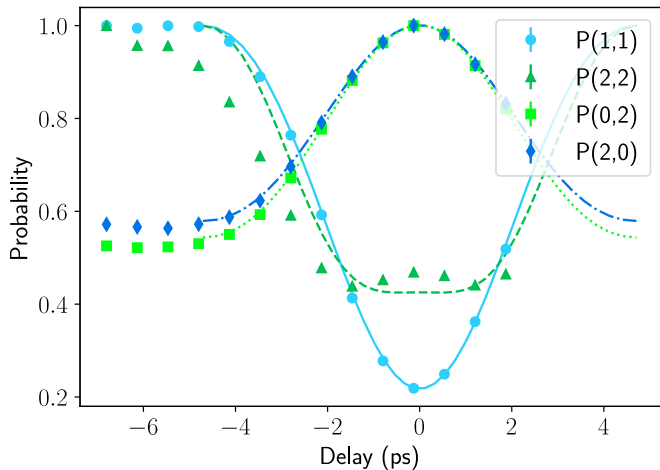


FIG. 4. Probability of individual photon number components normalized to maximum occurrence. Measured values from the joint photon number distributions, together with the respective probabilities from simulation.

can see that the measured joint photon number distributions are substantially different to the simulated lossless cases shown in FIG. 1 b) and c). This is due to the losses in the experiment eliminating the strict photon number correlations of the quantum state. The simulated joint photon number distributions, including experimental losses and matching the temporal delays of the measured ones in FIG. 3 b) and d), are shown in FIG. 3 c) and e), confirming that losses are the main cause for the difference to the ideal case in FIG. 1 b) and c).

In FIG. 4 we show four individual probabilities of having a specific number of photons in each output for the complete range of temporal delays measured. First we show the standard DVQO HOMI dip, the probability of having one photon in each output $P(1,1)$. This shows very good agreement with our simulation.

Second, we show the probability of having two photons in each output $P(2,2)$. Previous work has shown that there is an increase in probability at zero time delay [32] for this output pattern. In the measured $P(2,2)$ probability we see the expected increase of probability at zero time delay, which are not present in our simulation. However, the presence of multiple modes in the experiment increases the probability of having a $P(2,2)$ event at zero time delay [32]. Our simulations do not account for multimodedness, therefore, it is most likely that the increased probability in the measurement is caused by our slight multimodedness of the source and may indicate that this can be used as a measure for multimodedness.

Lastly, the probabilities of having two photons in either output and zero in the other $P(2,0)$ and $P(0,2)$ are presented. They are also often referred to as bunching peaks. One can clearly see a significant increase in occurrence of these two components towards perfect interference (zero time delay). This increase, together with the decrease in the $P(1,1)$ component, indicates the creation

of N00N-states at zero time delay [7].

One can more readily see the creation of the N00N-state by repeating the previous correlation analysis with a truncated joint probability distribution (see FIG. 5). For the truncation we remove all photon number components containing more than 2 photons and condition on the detection of at least one photon, removing the vacuum component. This describes the typical DVQO HOMI experiment. All three correlation measures show increased correlation at zero temporal delay compared to the values at large temporal delay and good agreement between simulation and measurement. Although, there is an offset for the Schmidt number between the measured values and our simulation, they follow the same trend. We see in our simulation that this offset is sensitive to the squeezing parameter and losses used, however, as these values are measured we keep them and accept the offset here. Note that the correlation coefficient is negative and therefore possesses a dip at zero time delay.

V. DISCUSSION

The observation of entangled N00N-states in the DVQO case brings us back to the apparent contradiction mentioned in the beginning, where both the DVQO and CVQO pictures can be correct in their interpretation of entanglement. CVQO considers the full infinite dimensional Hilbert space of all photon numbers, as CVQO looks at field quantities, which are captured only by the complete Hilbert space. DVQO traditionally considers the two photon subspace space by employing correlation measurements with click detectors. The key difference between the field measurements in CVQO and the photon counting measurements in DVQO is the conditioning of the photon counting measurements on having *at least one photon*, effectively removing the vacuum component $P(0,0)$ from the joint probability distribution. In fact, it can be shown that the action of the beam-splitter on the TMSVS does indeed produce two unentangled SMSVS. However, if we condition the state on the requirement that there is at least one photon found then the corresponding two-mode state is entangled. This conditioning is introducing correlated information about the two-mode state, which leads to the entanglement, see Appendix D for a more detailed explanation. It follows that the measurement of higher-order photon number components will not make the state separable when the $P(0,0)$ probability is removed. Therefore, the truncation to the two-photon subspace, together with the conditioning on the detection of at least one photon present, enables us to detect an entangled two-photon N00N-state. This clarifies the reason for the difference in entanglement interpretations between DVQO and CVQO, DVQO is conditioning on detecting at least one photon, where as CVQO is measuring the complete statistics.

As a final note, photon number resolved correlation measurement paired with the three types of correlation

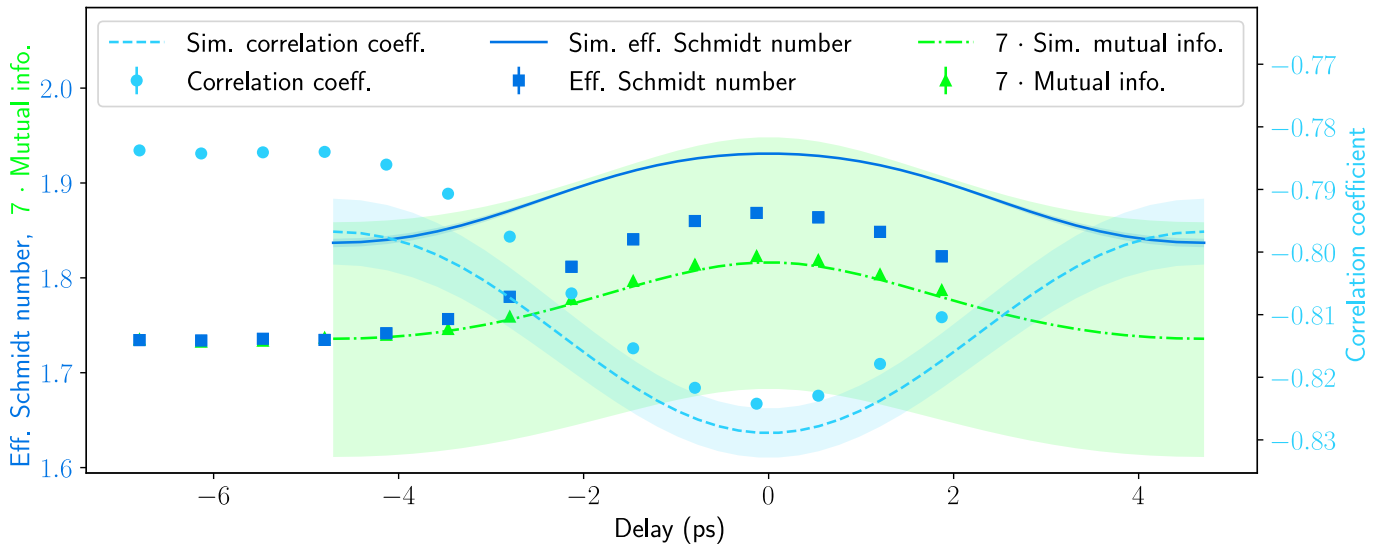


FIG. 5. Correlation measurements for two-photon subspace at different temporal overlaps of the input pulses.

measures enables us to accurately measure the amount of residual correlation after the transformation from TMSVS to SMSVS. With this we have a direct measure of the remaining correlations, improving upon the current practice of inferring the quality of the SMSVS by characterizing the TMSVS. Therefore, aiding in the development of sources for GBS and other hybrid applications.

VI. CONCLUSION

In this study we have taken a holistic approach to the interference of a TMSVS on a single beam splitter. Specifically, we have investigated the seeming contradiction between DVQO and CVQO with regards to the behavior of entanglement during the interference at a beam splitter. We did this by interfering a close to perfectly single spectral mode TMSVS generated by a type-II PDC source on a balanced beam splitter and measured the photon number correlations at different temporal overlaps of the two input modes from the TMSVS. We show that the CVQO as well as the DVQO interpretations are correct in their respective Hilbert spaces. CVQO considers the complete infinite-dimensional Hilbert space of the states where as DVQO traditionally considers the two-photon Hilbert space. The key difference here is that in the DVQO case the two-photon Hilbert space implies that the at least one photon is detected. This results in the interpretations of entanglement being correct in both fields even though at first glance they contradict each other. Therefore, the rather strict separation between CVQO and DVQO might need to be loosened with hybrid systems becoming more and more popular. Also, we propose this PNR correlation measurement for the characterization of SMSVS as a direct measure of the correlation in the ideally single spectral mode SMSVS

created from type-II PDC. Advancing the development of sources for hybrid applications.

ACKNOWLEDGMENTS

F.S. is part of the Max Planck School of Photonics supported by the German Federal Ministry of Education and Research (BMBF), the Max Planck Society, and the Fraunhofer Society. SMB is supported by the Royal Society (RSRP/R/210005). This work has received funding from the German Ministry of Education and Research within the PhoQuant project (Grant No. 13N16103) and from the European Commission through the Horizon Europe project EPIQUE (Grant No. 101135288).

Appendix A: Joint probability distributions

Here we describe how the joint probability distributions $P_{AB}(n_1, n_2)$ and $P_{CD}(n_1, n_2)$ from FIG. 1 b) and c) in the main text are obtained. We start from a TMSVS $|\psi\rangle_{\text{TMSVS}}$ [9]

$$|\psi\rangle_{\text{TMSVS}} = S_{AB}(\xi) |0\rangle_A |0\rangle_B \quad (\text{A1})$$

where $S_{AB}(\xi)$ is the two-mode squeezing operator (see Eq. (C1)) and $|0\rangle_{A(B)}$ is the vacuum state in modes A and B . In the photon number representation this state can be written as

$$|\psi\rangle_{\text{TMSVS}} = \frac{1}{\cosh r} \sum_{n=0}^{\infty} (-1)^n e^{in\phi} (\tanh r)^n |n\rangle_A |n\rangle_B. \quad (\text{A2})$$

The joint photon number distribution $P_{AB}(n_1, n_2)$ for this state is

$$P_{AB}(n_1, n_2) = |\langle n_1 | \langle n_2 | \psi \rangle_{\text{TMSVS}}|^2 = \begin{cases} (\cosh r)^{-2} (\tanh r)^{2n}, & \text{for } n_1 = n_2, \\ 0, & \text{for } n_1 \neq n_2. \end{cases} \quad (\text{A3})$$

This shows the perfect photon number correlation present in FIG. 1 b) in the main text.

It can be shown that the interference of a TMSVS on a balanced beam splitter results in

$$|\psi\rangle_{CD} = |\psi\rangle_{\text{SMSVS}, C} \otimes |\psi\rangle_{\text{SMSVS}, D} \quad (\text{A4})$$

with

$$\begin{aligned} |\psi\rangle_{\text{SMSVS}} &= \exp\left[\frac{1}{2}(\xi^* \hat{a}^2 - \xi \hat{a}^{\dagger 2})\right] |0\rangle \\ &= \frac{1}{\sqrt{\cosh r}} \sum_{n=0}^{\infty} (-1)^n \frac{\sqrt{(2n)!}}{2^n n!} \\ &\quad \cdot e^{in\phi} (\tanh r)^n |2n\rangle. \end{aligned} \quad (\text{A5})$$

The photon number probability for this state is given by

$$P(n) = |\langle n | \psi \rangle_{\text{SMSVS}}|^2 = \begin{cases} \frac{(2n)!}{2^{2n} (n!)^2} \frac{(\tanh r)^{2n}}{\cosh r}, & \text{for } n \text{ even,} \\ 0, & \text{for } n \text{ odd.} \end{cases} \quad (\text{A6})$$

The joint probability distribution of the state $|\psi\rangle_{CD}$ can then be written as

$$\begin{aligned} P_{CD}(n_1, n_2) &= \left| \langle n_1 | \langle n_2 | \psi \rangle_{\text{SMSVS}, C} \langle \psi |_{\text{SMSVS}, D} \right|^2 \\ &= \left| \langle n_1 | \psi \rangle_{\text{SMSVS}, C} \cdot \langle n_2 | \psi \rangle_{\text{SMSVS}, D} \right|^2 \\ &= \left| \langle n_1 | \psi \rangle_{\text{SMSVS}, C} \right|^2 \cdot \left| \langle n_2 | \psi \rangle_{\text{SMSVS}, D} \right|^2 \\ &= P_C(n_1) \cdot P_D(n_2), \end{aligned} \quad (\text{A7})$$

which shows the separability of the joint probability distribution shown in FIG. 1 c) of the main text.

Appendix B: Experimental Losses

The losses in the experiment were characterized using the Klyshko method [34]. We measured the transmission of the free space part of the experiment (from the source to the fiber coupling) without the fiber beam splitter and with the high efficiency detectors to be $35\% \pm 1\%$. Therefore, these are losses that happen before the interference at the beam splitter. This will be taken into account for the later simulations.

The losses of the two TMDs were also measured individually by measuring the Klyshko efficiency of the PDC

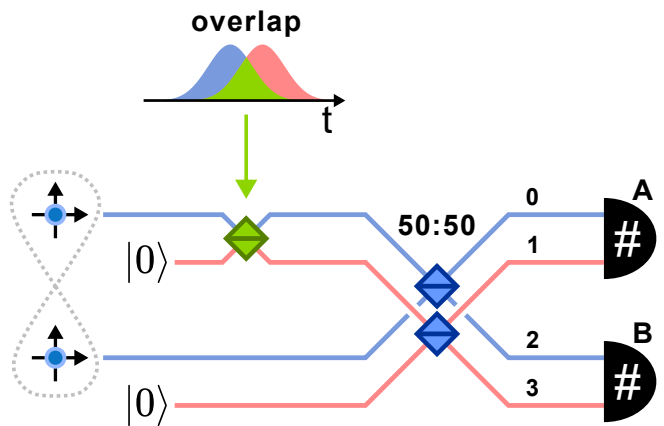


FIG. 6. Schematic depiction of the used theory model describing the multi-photon interference.

source before and after inserting the TMD. The difference between the initial efficiency and the efficiency with the TMD in the setup is the efficiency of the TMD. Both had similar efficiency of $60\% \pm 2\%$.

The detector efficiencies were measured using a laser and calibrated attenuators, where we measured the laser power with a power meter and attenuated it to the single photon level. From this we can get the expected number of photons at the detector and compare it to the measured number of clicks. The resulting detector efficiencies are $94\% \pm 6\%$ and $70\% \pm 6\%$, for the slow and fast detectors, respectively.

The TMD and the detector losses are the losses after the interference at the beam splitter. This will also be taken into account for the simulations.

From this we get the total transmission of the experimental setup of $20\% \pm 6\%$ and $14\% \pm 6\%$, for the high and low efficiency arm respectively.

Appendix C: Simulation

Here, we describe the theoretical model that we utilize to simulate the measured multi-photon interference effects reported in the main text. The initial state generated by a single-mode type-II PDC source in the high gain regime is a two-mode squeezed state which can be described by applying the operator

$$S_{ij}(\xi) = \exp\left(\xi^* \hat{a}_i \hat{a}_j - \xi \hat{a}_i^\dagger \hat{a}_j^\dagger\right) \quad (\text{C1})$$

to the vacuum. Here, $\xi = r \exp(i\phi)$ with r the squeezing parameter and ϕ the squeezing angle. i, j label the spatial modes to which the operator is applied. We only consider the case of $\phi = 0$, therefore, $\xi = r$. To model the interference of perfectly indistinguishable photons on a beam splitter we could just apply the unitary transfor-

mation

$$B_{ij}(\theta) = \exp\left(\theta \hat{a}_i \hat{a}_j^\dagger - \theta \hat{a}_i^\dagger \hat{a}_j\right) \quad (\text{C2})$$

to the corresponding spatial modes (with $\theta = \pi/4$ for a 50:50 splitter). However, to model the system including distinguishability we employ a 4-spatial mode model as depicted in FIG. 6. The indistinguishable case is modeled via spatial modes 0 and 2 (depicted in blue), where the total TMSVS is interfered on a 50:50 beam splitter. We utilize the additional spatial modes 1 and 3 (in red) to include the contribution of photons which do not interfere due to distinguishability. For introducing the distinguishability we transfer a part of the state in spatial mode 0 to spatial mode 1 by applying a beam splitter (see FIG. 6 green beam splitter). The splitting ratio of this beam splitter θ_{dis} is than mapped to the temporal delay from the experiment via the temporal overlap

$$\theta_{dis} = \int_{-\infty}^{\infty} dt f_s(t) f_i(t) \quad (\text{C3})$$

between the signal- and idler-fields $f_s(t)$ and $f_i(t)$, respectively. The portion of light that is coupled to spatial mode 1 is not interfered with the remaining TMSVS but split by a 50:50 beam splitter and evenly distributed to spatial modes 1 and 3. The total state before detection is then given by

$$|\Psi\rangle = B_{13}(\pi/4)B_{02}(\pi/4)B_{01}(\theta_{dis})S_{02}(r)|0\rangle. \quad (\text{C4})$$

To account for the fact that in the experiment the contributions of distinguishable and indistinguishable photons are detected on the same detectors we model the detection by assuming joint detection of spatial modes 0 and 1, as well as 2 and 3. For this we first calculate the probabilities

$$P(\mathbf{n}) = |\langle \mathbf{n} | \Psi \rangle|^2 \quad (\text{C5})$$

of detecting a photon number pattern $\mathbf{n} = (n_0, n_1, n_2, n_3)$ and then combine these via

$$P(n_A, n_B) = \sum_{\substack{n_B=n_0+n_1 \\ n_A=n_2+n_3}} P(\mathbf{n}) \quad (\text{C6})$$

to obtain the probability $P(n_A, n_B)$ of detecting n_A photons in detector A and n_B photons in detector B.

Appendix D: Conditioning effect

Here we show why conditioning on the detection of at least one photon, in the DVQO case, changes two separable SMSVS into an entangled state. To see this we start with the state of two SMSVS

$$|r\rangle_a | -r \rangle_b = \sum_{n,m=0}^{\infty} (-1)^m \frac{\sqrt{(2n)!(2m)!}}{n!m!} \cdot \left(\frac{\tanh r}{2}\right)^{n+m} |2n\rangle_a |2m\rangle_b, \quad (\text{D1})$$

where we neglect the normalization. The key point in our analysis is that this state will be modified if we have further information about it and that this information can leave the state entangled. There are two distinct types of information that we may have: *uncorrelated* and *correlated* information. It is fundamentally the difference between these that leaves the modified state separable or entangled. Let us consider each in turn.

1. Uncorrelated information

Uncorrelated information tells us something about the state of one of the modes or of them both but does not reveal any correlated or joint information. A simple example, appropriate for the small squeezing limit, is the statement that both modes have either two photons or are in their vacuum state. With this information, we must modify the state to remove all components in which either mode has four or more photons, with the result

$$|r\rangle_a | -r \rangle_b \rightarrow |0\rangle_a |0\rangle_b + \frac{\tanh r}{\sqrt{2}} (|2\rangle_a |0\rangle_b - |0\rangle_a |2\rangle_b) - \frac{\tanh^2 r}{2} |2\rangle_a |2\rangle_b. \quad (\text{D2})$$

This state is clearly separable

$$\left(|0\rangle_a + \frac{\tanh r}{\sqrt{2}} |2\rangle_a\right) \left(|0\rangle_b - \frac{\tanh r}{\sqrt{2}} |2\rangle_b\right) \quad (\text{D3})$$

and this is a consequence of the fact that the information added has told us nothing about the correlations between the modes.

2. Correlated information

It is a different story if the additional information is correlated, i.e. if it tells us something about the joint properties of the two modes. The simplest (and also most natural) example is if we know (or require) that there are at least some photons present. Equivalently, we can state that the two-mode state is then orthogonal to the two-mode vacuum state. It is essential to appreciate that this is indeed a correlated piece of information: we are not stating that either mode is in the vacuum state, but rather that only one of the two modes can be in its vacuum state. If we again ignore normalization then the state is modified as

$$|r\rangle_a | -r \rangle_b \rightarrow |r\rangle_a | -r \rangle_b - |0\rangle_a |0\rangle_b. \quad (\text{D4})$$

The simplest way to see that this is indeed entangled is to see what happens to the state of mode b when we measure the photon number in mode a . There are two distinct cases: In the first, if the measurement on mode a reveals the presence of photons, then mode b is left in the

state $| -r \rangle_b$. If, however, the measurement shows mode a to be in its vacuum state the state of mode b is modified to $| -r \rangle_b - | 0 \rangle_b$, i.e. the squeezed vacuum state without its vacuum component. The mere fact that we started with a pure two-mode state and that different measurement outcomes on mode a leave mode b in different states suffices to ensure that the initially separable two-mode state becomes entangled when modified by *correlated* informa-

tion.

We note that the truncation of the state by the removal of amplitudes corresponding to more than two photons (in each mode) does not, alone, suffice to produce an entangled state. To produce an entangled state we need this truncation to be in the form of correlated information as, for example, the statement that the two modes, between them, have precisely (or at most) two photons.

-
- [1] U. L. Andersen, J. S. Neergaard-Nielsen, P. van Loock, and A. Furusawa, Hybrid discrete- and continuous-variable quantum information, *Nature Physics* **11**, 713 (2015).
- [2] C. S. Hamilton, R. Kruse, L. Sansoni, S. Barkhofen, C. Silberhorn, and I. Jex, Gaussian boson sampling, *Physical Review Letters* **119**, 170501 (2017).
- [3] R. Kruse, C. S. Hamilton, L. Sansoni, S. Barkhofen, C. Silberhorn, and I. Jex, Detailed study of gaussian boson sampling, *Physical Review A* **100**, 032326 (2019).
- [4] H.-S. Zhong, H. Wang, Y.-H. Deng, M.-C. Chen, L.-C. Peng, Y.-H. Luo, J. Qin, D. Wu, X. Ding, Y. Hu, P. Hu, X.-Y. Yang, W.-J. Zhang, H. Li, Y. Li, X. Jiang, L. Gan, G. Yang, L. You, Z. Wang, L. Li, N.-L. Liu, C.-Y. Lu, and J.-W. Pan, Quantum computational advantage using photons, *Science* **370**, 1460 (2020).
- [5] L. S. Madsen, F. Laudenbach, M. F. Askarani, F. Rortais, T. Vincent, J. F. F. Bulmer, F. M. Miatto, L. Neuhaus, L. G. Helt, M. J. Collins, A. E. Lita, T. Gerrits, S. W. Nam, V. D. Vaidya, M. Menotti, I. Dhand, Z. Vernon, N. Quesada, and J. Lavoie, Quantum computational advantage with a programmable photonic processor, *Nature* **606**, 75 (2022).
- [6] C. K. Hong, Z. Y. Ou, and L. Mandel, Measurement of subpicosecond time intervals between two photons by interference, *Physical Review Letters* **59**, 2044 (1987).
- [7] J. P. Dowling, Quantum optical metrology – the low-down on high-n00n states, *Contemporary Physics* **49**, 125 (2008).
- [8] A. Eckstein, A. Christ, P. J. Mosley, and C. Silberhorn, Highly efficient single-pass source of pulsed single-mode twin beams of light, *Physical Review Letters* **106**, 013603 (2011).
- [9] S. M. Barnett and P. M. Radmore, *Methods in theoretical quantum optics* (Oxford University Press, Oxford, 1997).
- [10] A. Einstein, B. Podolsky, and N. Rosen, Can quantum-mechanical description of physical reality be considered complete?, *Physical Review* **47**, 777 (1935).
- [11] S. Takeda, K. Takase, and A. Furusawa, On-demand photonic entanglement synthesizer, *Science Advances* **5**, 10.1126/sciadv.aaw4530 (2019).
- [12] M. V. Larsen, X. Guo, C. R. Breum, J. S. Neergaard-Nielsen, and U. L. Andersen, Fiber-coupled epr-state generation using a single temporally multiplexed squeezed light source, *npj Quantum Information* **5**, 10.1038/s41534-019-0170-y (2019).
- [13] F. Yang, A. Tashchilina, E. S. Moiseev, C. Simon, and A. I. Lvovsky, Far-field linear optical superresolution via heterodyne detection in a higher-order local oscillator mode, *Optica* **3**, 1148 (2016).
- [14] M. D. Reid, P. D. Drummond, W. P. Bowen, E. G. Cavalcanti, P. K. Lam, H. A. Bachor, U. L. Andersen, and G. Leuchs, Colloquium: The einstein-podolsky-rosen paradox: From concepts to applications, *Reviews of Modern Physics* **81**, 1727 (2009).
- [15] D. Bouwmeester, ed., *The physics of quantum information*, 3rd ed., Physics and astronomy online library (Springer, Berlin, 2001) includes bibliographical references (p. [295] - 309) and index.
- [16] A. G. Asuero, A. Sayago, and A. G. González, The correlation coefficient: An overview, *Critical Reviews in Analytical Chemistry* **36**, 41 (2006).
- [17] A. Ekert and P. L. Knight, Entangled quantum systems and the schmidt decomposition, *American Journal of Physics* **63**, 415 (1995).
- [18] C. K. Law, I. A. Walmsley, and J. H. Eberly, Continuous frequency entanglement: Effective finite hilbert space and entropy control, *Physical Review Letters* **84**, 5304 (2000).
- [19] B. Brecht, D. V. Reddy, C. Silberhorn, and M. Raymer, Photon temporal modes: A complete framework for quantum information science, *Physical Review X* **5**, 041017 (2015).
- [20] T. M. Cover, *Elements of information theory*, second edition ed., edited by J. A. Thomas (Wiley-Interscience, Hoboken, N.J, 2006) includes bibliographical references (pages 689-721) and index.
- [21] F. Pegoraro, P. Held, S. Barkhofen, B. Brecht, and C. Silberhorn, Dynamic conditioning of two particle discrete-time quantum walks, *Physica Scripta* **98**, 034005 (2023).
- [22] G. Harder, T. J. Bartley, A. E. Lita, S. W. Nam, T. Gerrits, and C. Silberhorn, Single-mode parametric-down-conversion states with 50 photons as a source for mesoscopic quantum optics, *Physical Review Letters* **116**, 143601 (2016).
- [23] A. Christ, K. Laiho, A. Eckstein, K. N. Cassemiro, and C. Silberhorn, Probing multimode squeezing with correlation functions, *New Journal of Physics* **13**, 033027 (2011).
- [24] M. Avenhaus, K. Laiho, M. V. Chekhova, and C. Silberhorn, Accessing higher order correlations in quantum optical states by time multiplexing, *Physical Review Letters* **104**, 063602 (2010).
- [25] E. Meyer-Scott, N. Montaut, J. Tiedau, L. Sansoni, H. Herrmann, T. J. Bartley, and C. Silberhorn, Limits on the heralding efficiencies and spectral purities of spectrally filtered single photons from photon-pair sources, *Physical Review A* **95**, 061803 (2017).
- [26] D. Achilles, C. Silberhorn, C. Śliwa, K. Banaszek, and I. A. Walmsley, Fiber-assisted detection with photon number resolution, *Optics Letters* **28**, 2387 (2003).
- [27] J. Tiedau, C. Silberhorn, and T. Bartley, *Quantum optics*

- in the photon number basis* (Paderborn, 2020).
- [28] R.-B. Jin, T. Gerrits, M. Fujiwara, R. Wakabayashi, T. Yamashita, S. Miki, H. Terai, R. Shimizu, M. Takeoka, and M. Sasaki, Spectrally resolved hong-ou-mandel interference between independent photon sources, *Optics Express* **23**, 28836 (2015).
- [29] T. Kobayashi, R. Ikuta, S. Yasui, S. Miki, T. Yamashita, H. Terai, T. Yamamoto, M. Koashi, and N. Imoto, Frequency-domain hong-ou-mandel interference, *Nature Photonics* **10**, 441 (2016).
- [30] D. Achilles, C. Silberhorn, C. Sliwa, K. Banaszek, I. A. Walmsley, M. J. Fitch, B. C. Jacobs, T. B. Pittman, and J. D. Franson, Photon-number-resolving detection using time-multiplexing, *Journal of Modern Optics* **51**, 1499 (2004).
- [31] S. Krishnaswamy, F. Schlue, L. Ares, V. Dyachuk, M. Stefszky, B. Brecht, C. Silberhorn, and J. Sperling, Experimental retrieval of photon statistics from click detection, *Physical Review A* **110**, 023717 (2024).
- [32] A. Ferreri, V. Ansari, C. Silberhorn, and P. R. Sharapova, Temporally multimode four-photon hong-ou-mandel interference, *Physical Review A* **100**, 053829 (2019).
- [33] A. Lyons, G. C. Knee, E. Bolduc, T. Roger, J. Leach, E. M. Gauger, and D. Faccio, Attosecond-resolution hong-ou-mandel interferometry, *Science Advances* **4**, 10.1126/sciadv.aap9416 (2018).
- [34] D. N. Klyshko, Use of two-photon light for absolute calibration of photoelectric detectors, *Soviet Journal of Quantum Electronics* **10**, 1112 (1980).